Department of Inorganic Chemistry
Fritz-Haber-Institut der MPG

Freie Universität Berlin

Novel Cu/ZnO Catalyst Precursors for Synthesis of Methanol

Felix Hermerschmidt

Novel Cu/ZnO Catalyst Precursors for Synthesis of Methanol

von
Felix Hermerschmidt
aus Berlin

Institut für Chemie und Biochemie
des Fachbereichs Biologie, Chemie, Pharmazie
der Freien Universität Berlin

zur Erlangung des Hochschulgrades
Bachelor of Science
B.Sc.

vorgelegte Bachelorarbeit

angefertigt am
Fritz-Haber-Institut der Max-Planck-Gesellschaft

Erstbetreuer: Prof. Dr. R. Schlögl, Fritz-Haber-Institut
Zweitbetreuer: Prof. Dr. J. Beckmann, Freie Universität Berlin

Berlin, September 2009

Erklärung zur Bachelorarbeit/Declaration of Authorship

Hiermit bestätige ich, dass ich die vorliegende Bachelorarbeit mit dem Thema **Novel Cu/ZnO Catalyst Precursors for Synthesis of Methanol** ausschließlich unter Zuhilfenahme der in der Arbeit angegebenen Quellen angefertigt habe.

I hereby declare that the paper I am submitting under the title **Novel Cu/ZnO Catalyst Precursors for Synthesis of Methanol** is entirely my own work except where references indicate otherwise.

Berlin, 4/9/2009 ……

Felix Hermerschmidt

List of Figures

Table of Contents

1 Introduction

Methanol is one of the most important basic chemicals in chemical industry. Its annual production was around 47 million tons in 2008 [1]. The main industrial applications for methanol are to produce other basic chemicals such as formaldehyde, methyl *tert*-butyl ether (MTBE) and acetic acid (see Figure 1.1).

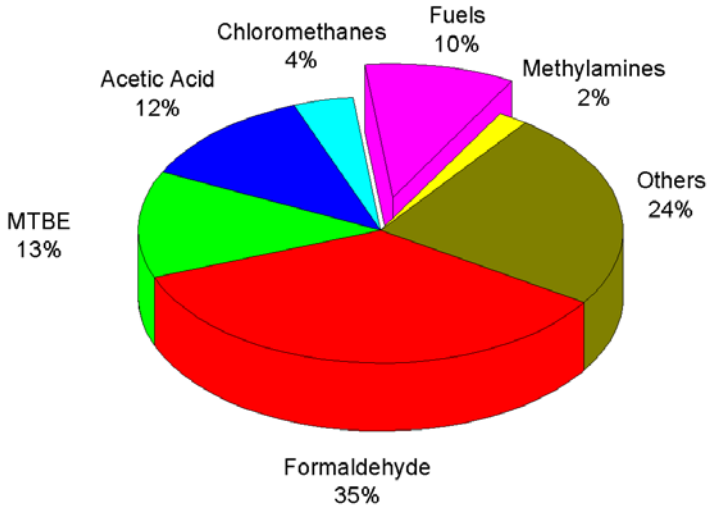

Figure 1.1: Industrial applications of methanol in 2008

Fuels make up around 10 % of the overall applications of methanol and this figure has been steadily rising over the past few years and looks likely to continue to rise as discussions about "clean" and "green" fuels increase.

Methanol is a compact molecule with high energy content (173.6 kcal/mol) and can act as a potential chemical hydrogen-carrier. 1 l of methanol contains more hydrogen than liquid hydrogen itself [2]. Because methanol is liquid at room temperature it offers better transport and storage properties – also in cold regions due to the low freezing point of -97.6 °C [3]. However, due to the polar character of methanol, some of the materials currently used for transportation and storage of petrol are not suitable for use with methanol [2].

A further advantage of methanol are its combustion properties in engines, which produce almost no harmful by-products such as SO_x or NO_x. The application in fuel cells is not restricted to conventional hydrogen-based types but direct methanol fuel cells are possible. However, impurities such as CO produced during reaction in the fuel cell have to be removed to prevent affecting cell performance as the electrodes deteriorate [4].

The compromise that has to be found in chemical industry is the use of methanol for the production of other basic chemicals as discussed earlier and its sole use as fuel, which offers independence from fossil sources of energy.

In industry, methanol is produced from H_2, CO and CO_2 – synthesis gas. These gases react in the presence of $Cu/ZnO/Al_2O_3$ catalytic systems, temperatures of 250 – 350 °C and pressures of up to 100 atm. Modern production plants achieve up to 5000 tons per day. The synthesis of methanol from synthesis gas is exothermic and accompanied by decreasing entropy. Therefore, low reaction temperatures and high reaction pressures are preferable. Synthesis occurs according to:

$$CO + 2\ H_2 \rightleftharpoons CH_3OH \tag{2.1}$$

$$CO_2 + 3\ H_2 \rightleftharpoons CH_3OH + H_2O \tag{2.2}$$

and combustion according to:

$$CH_3OH\ + 0.5\ O_2 \rightleftharpoons CO_2 + 2\ H_2 \tag{2.3}$$

The hydrogenation step can occur on both carbon monoxide and carbon dioxide. As can be seen in (2.2) and (2.3) the production and use of methanol is a “climate neutral” reaction – the carbon monoxide used in the reaction is re-emitted during combustion. Other promising synthesis routes start with methane (oxidation) or pure carbon dioxide (reduction). Both substances are known as “greenhouse gases” and the possibility to economically convert them is strongly desired [5].

2 Synthesis of Methanol

2.1 Industrial Catalysis

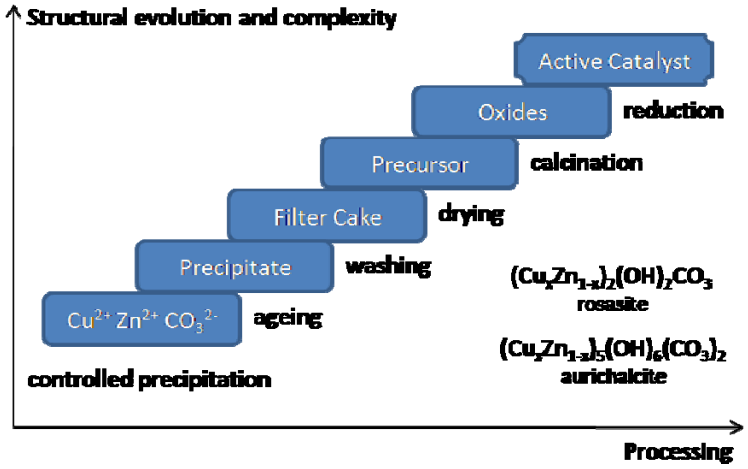

Figure 2.1: Industrial catalyst preparation procedure

The industrial catalyst currently in use is a 60:30:10 mixture of copper, zinc and aluminium. Al_2O_3 serves as structural promoter and improves the thermal stability of the catalyst [6]. ZnO acts not only as support and stabiliser but also as provider of active centres in presence of Cu. This effect is carried out by oxygen defect positions caused by the slightly reducing atmosphere. This results in a beneficial electronic structure for adsorption of reactants and products [7].

In academia, binary Cu/ZnO model catalysts are usually studied in order to reduce the complexity of the system. A general schema of industrial multi-step preparation of $Cu/ZnO/(Al_2O_3)$ catalysts is shown in Figure 2.1; adapted from [8]. The properties of the co-precipitated precursor material are of special importance, as they pre-determine the catalytic performance of the final catalyst. This phenomenon is denoted the "chemical memory" of the CuZnAl system [8]. Mixed basic carbonate precursors have proven to lead to highly active catalysts and are currently used in industry.

The benefit of the carbonate precursor route can be rationalised from the schema shown in Figure 2.2. In the first steps (co-precipitation, ageing, washing, drying) a typical needle-like basic carbonate – zincian malachite, $(Cu,Zn)_2(OH)_2CO_3$ – is formed, which contains both metal species in a joint cationic sublattice and decomposable anions (hydroxide, carbonate). Due to the fact that the monoxides CuO and ZnO are not or only very poorly dissolvable into each other, an arrangement of CuO and ZnO nanoparticles is formed by mild calcination of such kind of precursor. In the final step of the preparation, the more noble CuO component is reduced to yield the unique microstructure of Cu/ZnO catalysts: an alternating arrangement of active Cu nanoparticles with ZnO spacers to prevent them from sintering. Cu surface areas of industrial catalysts obtained by this method are as high as 30 - 40 m^2/g.

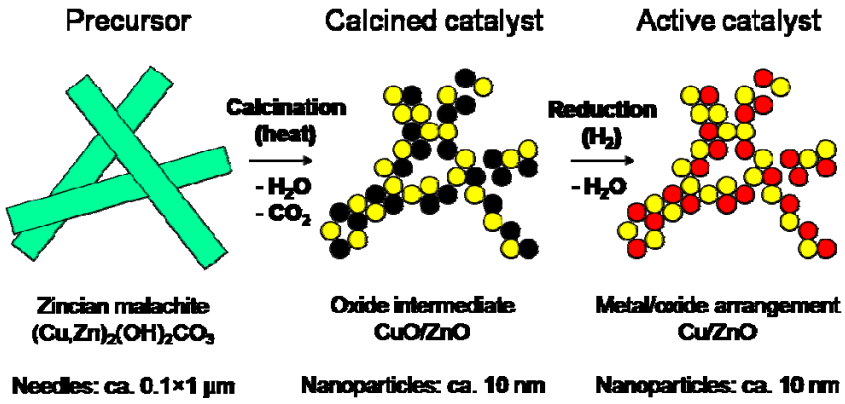

Figure 2.2: Schema of the microstructural development of Cu/ZnO catalyst at the different stages of preparation

It is obvious from Figure 2.2 that alternative precursors for Cu/ZnO catalysts, such as are investigated in this paper, must fulfil certain requirements if this general schema of nano-structuring successfully applied to carbonate precursors shall be transmitted to novel precursor systems. These general requirements are:

- The precursor should have volatile anions to be transformed into the oxides by calcination at low temperature without pronounced sintering of the newly formed particles.
- The precursor should have a homogeneous distribution of Cu and Zn, preferably within a joint cationic lattice, to guarantee an effective nano-structuring upon calcination.

- The precursor should have a high surface-to-volume ratio (high surface area, small particle size) to yield Cu nanoparticles, which are accessible to the reactant gas phase and not buried in the bulk of the catalyst.
- The precursor should have a Cu:Zn ratio near unity, because a maximum dispersion of CuO (and ZnO) can be expected for such a composition.

2.2 Current Research Activities

Current research into catalysts for use in the synthesis of methanol includes optimising the dispersion present in the catalyst precursor in order to increase the available Cu surface area in the final catalyst. Due to the "memory effect" discussed earlier there is a link between reaction parameters, the structure of the catalyst precursor and its active surface area, which has to be studied and understood in order to achieve controlled catalyst preparation. In general, the aim of precursor preparation should be to fulfil the requirements described in section 2.1.

2.3 Motivation behind Formate Series

Methanol has the potential of becoming an important chemical in terms of securing the world's energy problems, especially as it is seen as a "green" source of fuel if prepared from biomass or exhaust gas derived carbon dioxide and solar hydrogen. However, the current method of catalyst production could be "greener" since nitrate solutions are used for co-precipitation and make up the anionic part of the mother liquor that is then discarded. Formate as an anion has a better ecological footprint and concentrated formate solutions in waste water are less harmful to the environment than nitrate solutions.

Furthermore, there is a general interest in alternative anions to explore their potential for catalyst optimisation. So far, only little attention has been paid to the anionic parts of the starting salt solutions and the precursor material. Through different coordination properties and acid-base chemistry, the anions may be able to alter the physico-chemical properties of the precipitate in a way which is beneficial for the final catalyst.

In course of previous studies investigating co-precipitation of Cu/Zn precursors by titration experiments a new compound was discovered, which was identified as a mixed basic formate $(Cu,Zn)_2(OH)_3HCOO$ [9]. This compound fulfils the first two requirements for a Cu/ZnO catalyst precursor (cf. section 2.1) and, thus, can be seen as a promising candidate for further investigations. This work will explore the potential of this novel material using a combined preparation and characterisation approach as described in the next section 2.4.

2.4 Experimental Approach

A series of five experiments across the range of Cu:Zn mol% ratios, i.e. 100:0, 75:25, 50:50, 25:75, 0:100 were examined. The purpose behind this series was to analyse the maximum solubility of Zn^{2+} in the precursor phase and to show what effect the substitution of Cu with Zn had on the precursor's structure and subsequently also on the calcined and reduced materials.

A range of analytical techniques was used to examine the various experimental stages: X-ray diffraction (XRD) to analyse the crystal structure; X-ray fluorescence (XRF) and energy dispersive X-ray spectroscopy (EDX) to determine elemental composition; Brunauer, Emmett, Teller (BET) method for surface area analysis; thermogravimetric and evolved gas analysis (TG-EGA) to simulate the effects of calcination; temperature-programmed reduction (TPR) to reduce the copper oxides to active copper; scanning electron microscopy (SEM) and transmission electron microscopy (TEM) to show micrograph images of the samples.

3 Results and Discussion

3.1 The Precursor Material

Figure 3.1 shows the XRD patterns of the complete series of precursor samples. Prominent is the peak at 13.3 °2θ indicating that the target phase is present in the precipitated product. It can be identified as the (001) reflection of the monoclinic cell of a copper, zinc hydroxy formate, $Cu_2(OH)_3HCOO$, analogous to the isomorphous basic nitrate phase gerhardtite, $Cu_2(OH)_3NO_3$. This peak, however, is not visible in the zinc-only sample (0:100) indicating that a 100 % zinc phase is not accessible by the used co-precipitation synthesis. In general, this sample does not show much crystallinity at all and will therefore not be discussed further in the course of this paper. The focus will lie on the range of copper samples with increasing zinc content and primarily on the most promising of these with nominal 25:75 Cu:Zn content.

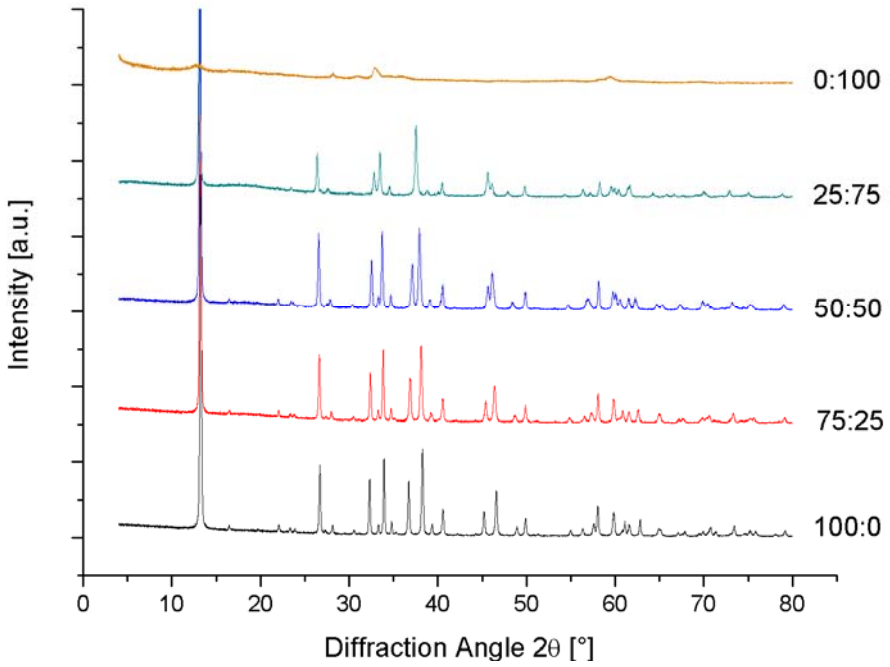

Figure 3.1: XRD patterns of precursor samples

As the close-up of the 30 - 40 °2θ range in Figure 3.2 shows, an increase in zinc content has an influence on the crystal structure of the samples. The peaks in the 100:0 sample at 32.3 °2θ and 33.9 °2θ as well as at 36.7 °2θ and 38.3 °2θ move closer together as the series progresses and even overlap in the nominal 25:75 sample. This is due to the change in plane distances as more Cu^{2+} ions are substituted by Zn^{2+}. As opposed to Cu^{2+} (d^9 configuration), Zn^{2+} ions (d^{10}) are not Jahn-Teller ions. As a result, the interatomic distances change significantly with increasing zinc content despite the similar ionic radii. CuO_6 octahedra show elongation of the axial O-Cu-O distances, while ZnO_6 octahedra, on the other hand, are not elongated and thus induce changes in the crystal structure of the mixed metal hydroxy formate system.

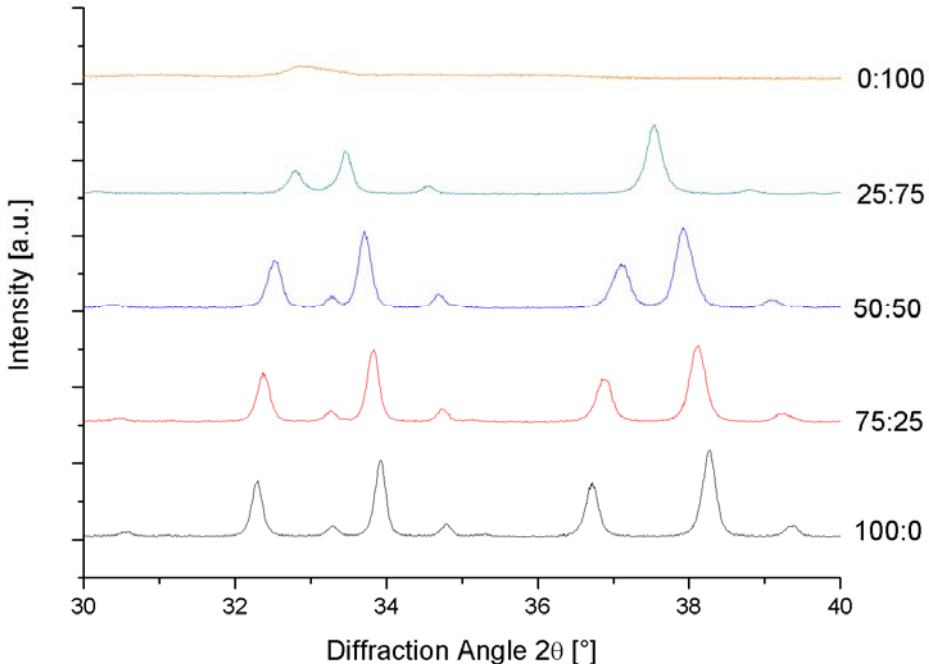

Figure 3.2: Detail of XRD patterns of precursor samples

Figure 3.3 shows the unit cell of the copper formate precursor seen along the b-axis when refined with the Rietveld method using the 100:0 XRD pattern and the known basic nitrate gerhardtite as a structural model, which is shown for comparison [10]. The monoclinic angle β changes the more copper is substituted by zinc (see Figure 3.4). The difference in β between the zinc-free and the zinc-richest sample is approximately 2.3°, too small a change to be shown in a series of still images. Linear changes in lattice parameters are usually observed in isomorphous substitution series

(Vegard's law) and the trend shown in Figure 3.4 is a clear proof of a partial dissolution of Zn in a joint cationic lattice in the basic formate precursor.

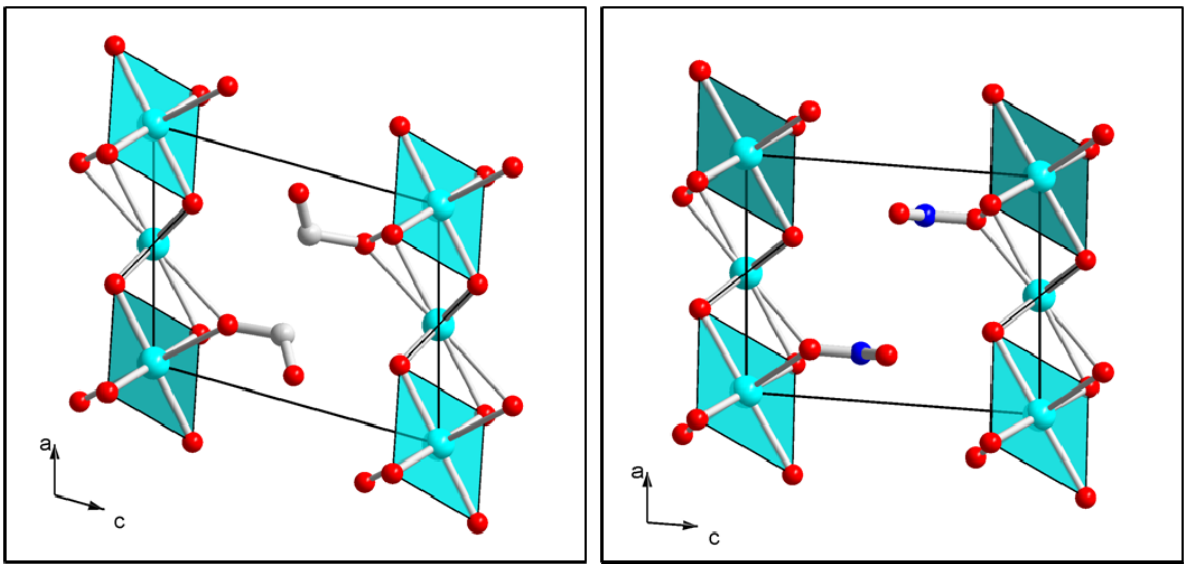

Figure 3.3: Monoclinic angle β; left: in formate system, right: in gerhardtite.

However, these changes in β are not directly connected to the change in octahedra shape but rather to the fact that the change in octahedra shape makes the formate anions alter their position in the matrix. It is the way the anions are positioned that determines the unit cell build-up. The formate anions are pointed away from each other (the central carbon's proton is not shown) while in gerhardtite the nitrate anions are parallel to one another. In malachite – the industrially applied precursor – on the other hand, the effects of zinc substitution are directly connected to the change that the MO_6 octahedra undergo as more zinc enters the crystal lattice. This is due to the difference in connectivity: The building units are three-dimensionally connected in malachite, while the basic formate precursor is a two-dimensional layered compound which allows more flexible orientation of the inter-layer anions.

It is noted that the excellent quality of the Rietveld fit, which is characterised by an R_{Bragg} factor of 4 %, leaves almost no doubt as to the analogy of the basic formate precursor and gerhardtite concerning composition and crystal structure.

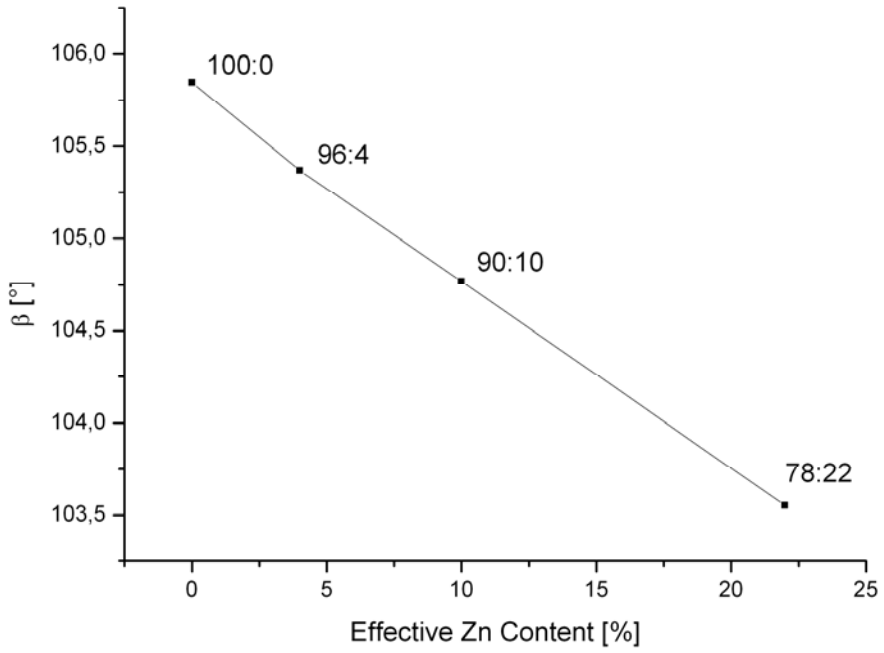

Figure 3.4: Change of monoclinic angle β as a function of zinc content

Table 3.1 shows the chemical composition of the five samples as obtained from XRF. There is a striking discrepancy between the nominal Cu:Zn ratios of the starting formate solutions and the measured ones. All mixed samples were found to be poor in Zn indicating that during co-precipitation not all of the metal ions were solidified and much Zn^{2+} remained dissolved in the mother liquor. However, there is a clear systematic correlation between the nominal and measured ratios and the nominally zinc-richest sample also shows the highest measured zinc content. As reported in [8] and [11], there seems to be a maximum amount of zinc capable of substituting copper in the matrix of the industrially applied basic carbonate precursor of around 28 %. This series' maximum value was at 22 % in the most promising sample; however, more could possibly be substituted with increasing nominal ratio or, preferably, with optimised synthesis parameters. Since neither copper nor zinc precipitated completely at the pH chosen for this series, these figures cannot be deemed particularly conclusive. Even so, the Cu/Zn system seems to still work in the same way in that a certain maximum amount of zinc is included in the copper matrix.

Nominal Cu:Zn Ratio	Effective Cu:Zn Ratio
100:0	100:0
75:25	96:4
50:50	90:10
25:75	78:22
0:100	0:100

Table 3.1: Precursor XRF Data

Figure 3.5 shows SEM micrographs of the zinc-richest sample of the series. Clearly visible are needle-like crystallites of about 1 µm length and 0.2 µm thickness. The XRF analyses are confirmed by EDX measurements and BET surface area analysis shows a value of 20 m^2/g. Good homogeneity is achieved.

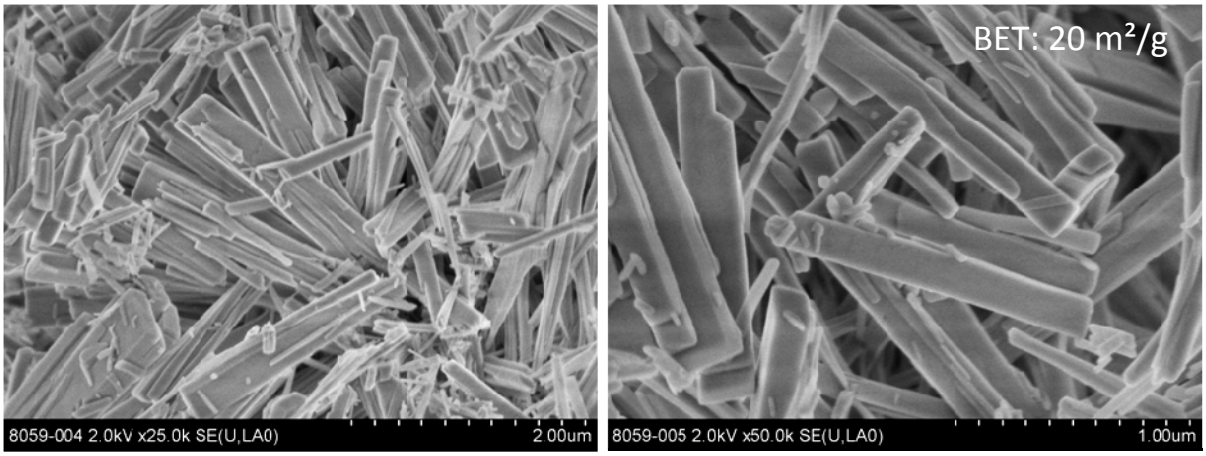

Figure 3.5: SEM micrographs of 78:22 precursor sample

The precursors' thermal properties were investigated by TG-EGA measurements in flowing synthetic air (21 % O_2/Ar) to simulate the conditions of calcination. The graphs in Figure 3.6 show how the relevant samples undergo the calcination process. Additionally, normalised graphs show at what temperature water and carbon dioxide are emitted. The overall mass loss of the 100 % Cu sample is 31.1 %, which is close to the theoretical value of 28.7 %, assuming CuO and ZnO are the only decomposition products. This agreement also confirms the proposed composition of the basic formate precursors in analogy to gerhardtite. The samples can be divided into two

groups: The 100 % and 96 % Cu samples essentially decomposed in one step at temperatures below 220 °C and slightly gain in weight in the temperature range 200 - 400 °C, while for the 90 % and 78 % Cu samples an additional decomposition step is observed at 399 °C and 442 °C, respectively. Several thermal events seem to contribute to the early decomposition step as indicated by the presence of many, not simultaneously appearing peaks in the MS traces. These contributions can be assigned to thermal dehydroxylation of the OH-groups evolving H_2O and burning of the formate anions yielding CO_2 and additional H_2O.

The second decomposition step present in the TG curves of the Zn-richer samples is a pure decarbonation as only CO_2 and no H_2O is emitted. The development of the TG curve in the series shows that the higher the zinc content included in the sample the higher the temperature of complete decarbonation.

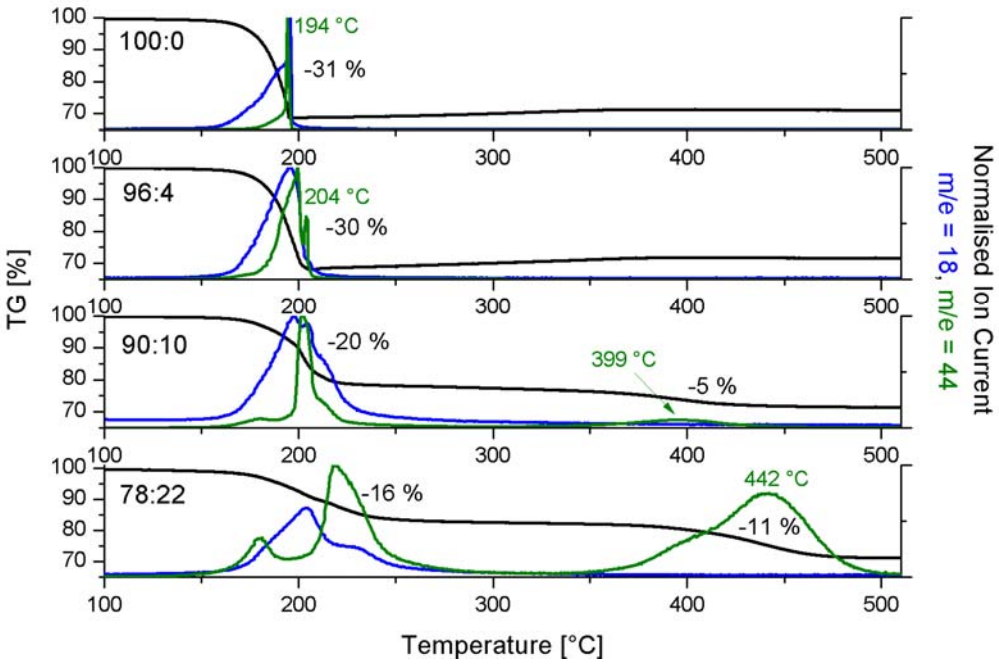

Figure 3.6: TG-EGA analyses of precursor samples

This so-called “high temperature carbonate” is commonly observed in synthetic carbonate precursors for Cu/ZnO catalysts prepared by co-precipitation [8,12]. The presence of these carbonates has been found to be a function of the Cu:Zn ratio and seems to be indicative of good catalytic properties of the prepared catalysts [13]. In

well-mixed precursors no large crystals of CuO or ZnO are formed after calcination. Instead, there are many interfaces and grain boundaries between CuO and ZnO domains. Because there is no crystalline order within the anionic lattice at these grain boundaries, they provide a place for the carbonate to be bound inside the material matrix. Thus, the presence of high temperature carbonates indicates a successful nano-structuring during calcination. In other words, the higher the temperature the sample needs to be to emit the final carbonate the higher the thermal stability of the nano-particulate arrangement of the oxide particles.

In the case of the initially carbonate-free basic formate precursors, CO_2 produced during decomposition of the formate anions seems to re-chemisorb on the oxide material to form stable carbonates if enough adsorption sites are present in the nano-structured material. According to these considerations, the Zn-richest sample, again, seems to represent the most promising catalyst precursor. Therefore, in the remainder of this paper the focus will lie on this sample, serving as a prototype for the basic formate precursor system.

3.2 The Calcined Material

Based on the TGA experiments (see previous section 3.1), a calcination temperature of 225 °C was used. Ideally, calcination should take place at a temperature that is as low as possible to hinder pronounced sintering and as high as necessary to decompose the major fraction of the anions.

SEM micrographs of the resulting Zn-richest sample after calcination in air and the respective elemental mapping can be seen in Figure 3.7 and Figure 3.8. The needle-like shape of the precursor particles can still be seen after calcination. At higher magnification one can see that the individual needles have decomposed to porous aggregates of much smaller particles. This as well as the increase in surface area from 20 m^2/g to 35 m^2/g indicates successful nano-structuring of most of the precursor according to the schema introduced in section 2.1. However, also larger particles with clearly developed crystal surfaces have been formed. Figure 3.8 shows that these particles are either rich in Cu or Zn and poor in the other element, indicating an undesired partial segregation of Cu and Zn during calcination.

This is confirmed by the XRD pattern of the sample after calcination in air shown in Figure 3.9. Narrow peaks of well-crystalline Cu_2O and ZnO are observed in addition to broadened reflections of CuO. Due to the difference in line width, the segregated large particles observed in SEM are assigned to Cu_2O and ZnO, while the highly dispersed Cu phase seems to be present as CuO.

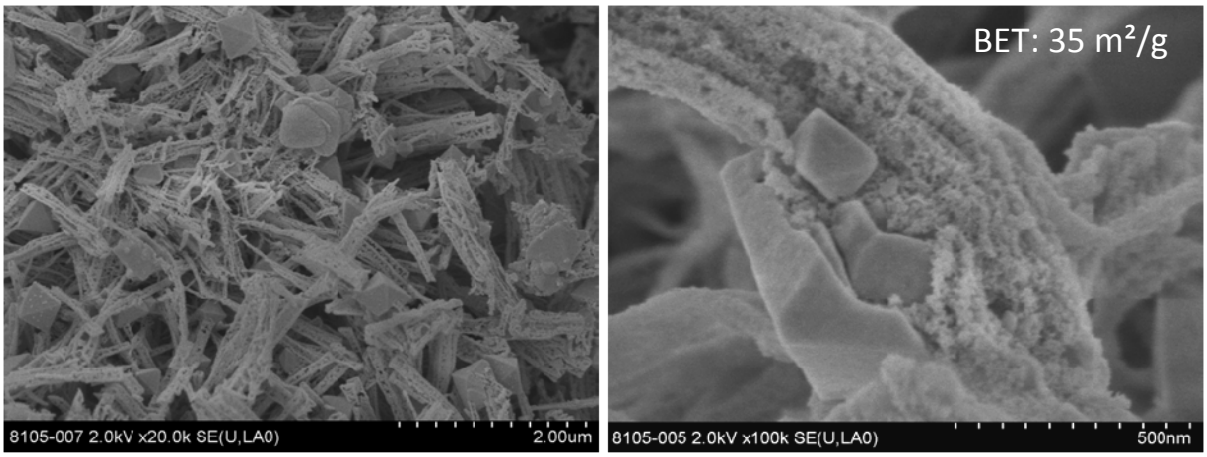

Figure 3.7: SEM micrographs of 78:22 sample calcined in air

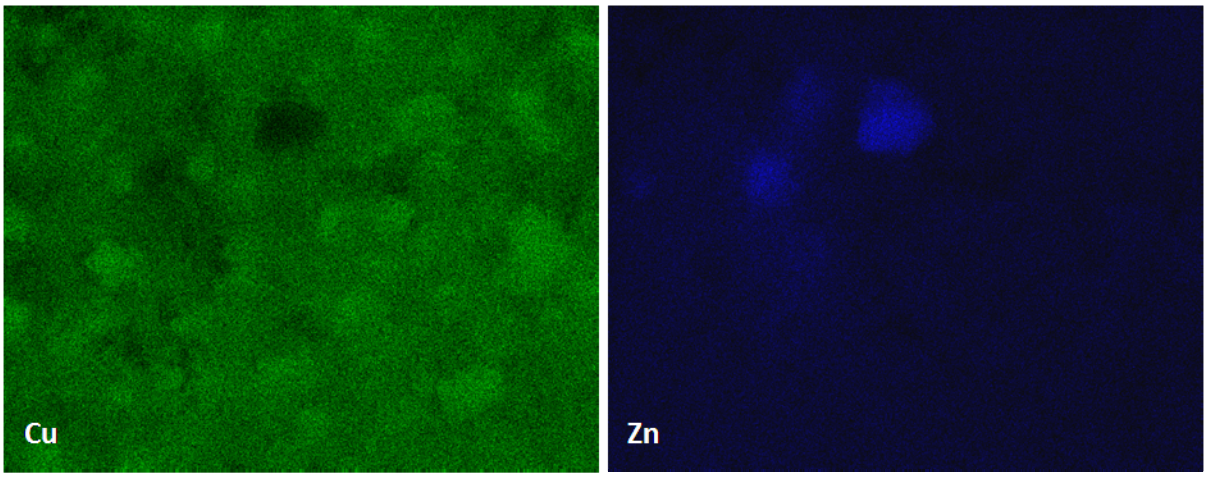

Figure 3.8: Elemental mapping of left-hand SEM micrograph in Figure 3.7

It can be concluded from this assignment that during calcination not only oxygen from air but also a fraction of copper was reduced from Cu(II) to Cu(I) upon oxidation of formate to CO_2. The presence of Cu_2O also explains the intermediate weight gain observed in the TG curves as Cu_2O is gradually transformed into CuO by oxygen uptake. Obviously, the internal reduction of Cu(II) is detrimental for catalyst preparation, because Cu_2O forms large crystals and destroys the homogeneous

distribution of Cu and Zn. In order to hinder this internal redox process, the calcination was repeated in a 100 % O_2 atmosphere instead of air. The higher partial pressure of oxygen leads to an increase in oxidising power of the atmosphere and should favour the reduction of oxygen over the reduction of Cu(II).

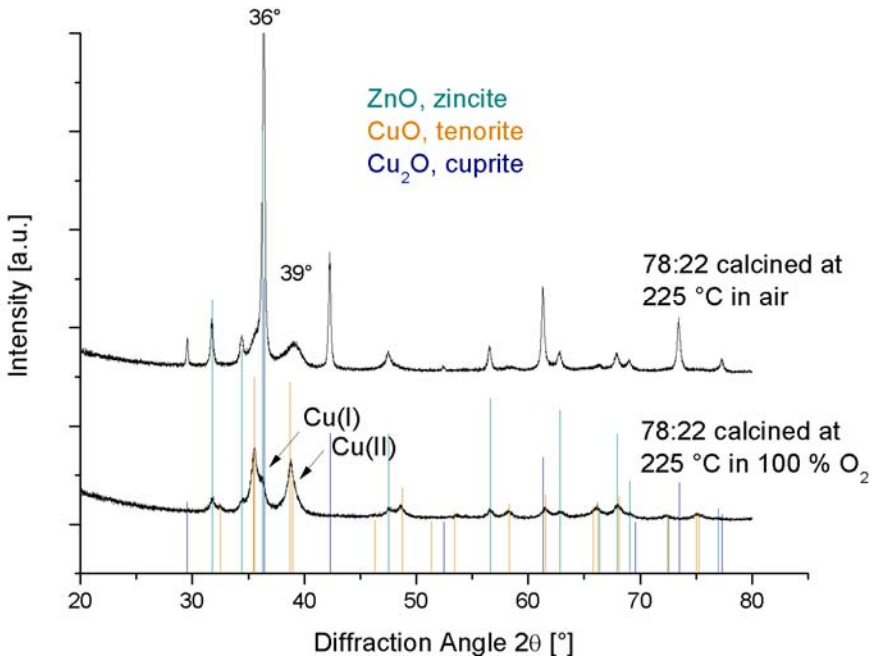

Figure 3.9: Comparison of XRD phases of 78:22 samples calcined in air and in 100 % oxygen

Figure 3.10 and Figure 3.11 show results of SEM and elemental mapping of the resulting sample. No large particles are observed in the micrographs, which show the needle-shaped aggregates as the only type of material. No indications of segregation can be observed and the metal distribution is homogeneous as shown by elemental mapping. The higher surface area of 40 m^2/g can also be explained with the absence of large particles.

The XRD pattern of the sample (see Figure 3.9) shows only ZnO and broad reflection of CuO, but no Cu_2O, indicating that the sample is generally less crystalline and consists of smaller particles. Overall, it is clear that calcination in 100 % oxygen suppresses the reduction of Cu(II) and provides the more promising sample. The surface area is higher, the homogeneity is greater and the sample's make-up finer.

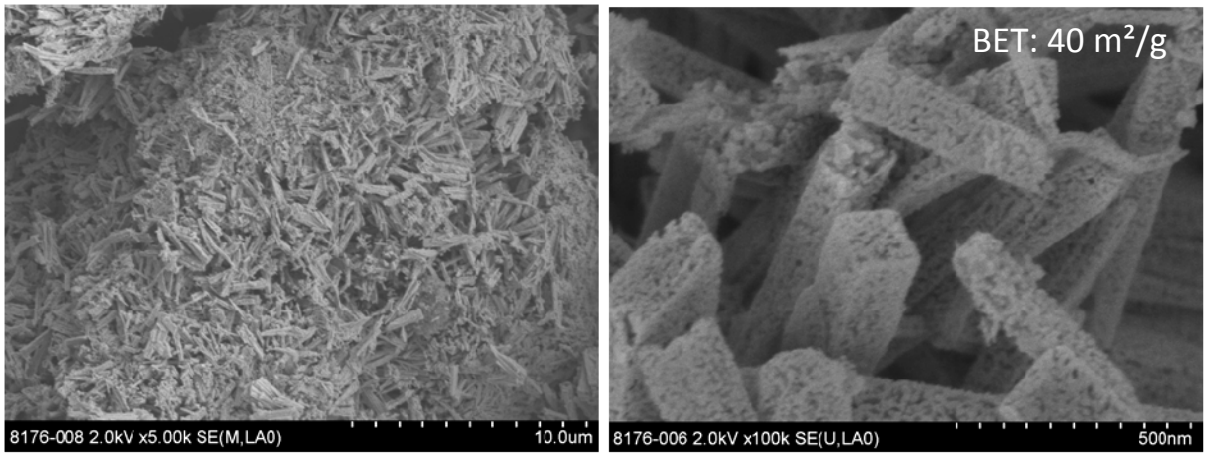

Figure 3.10: SEM micrographs of 78:22 sample calcined in 100 % oxygen

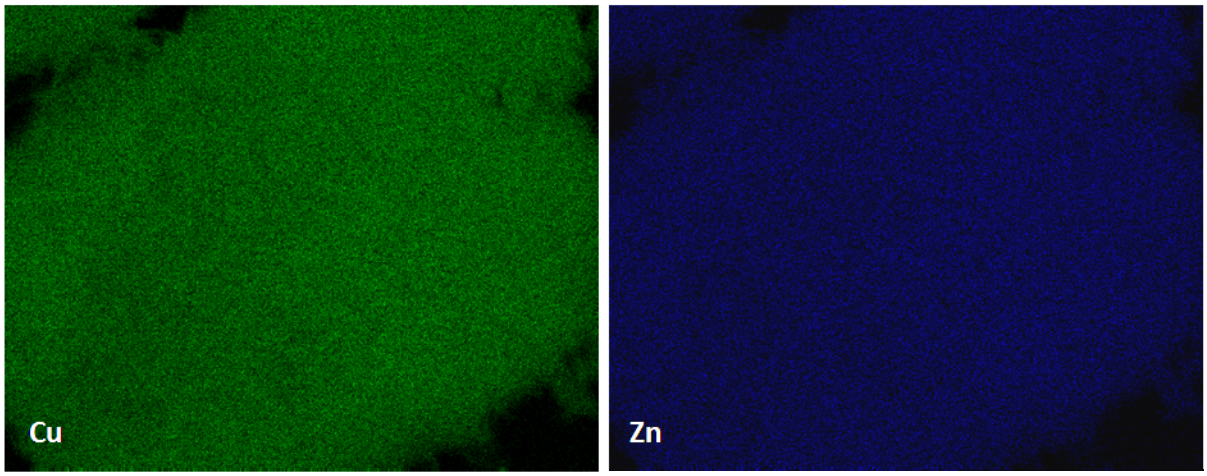

Figure 3.11: Elemental mapping of left-hand SEM micrograph in Figure 3.10

3.3 The Reduced Material

The calcination process is followed by reduction of the metal oxides to the active metal by TPR. Figure 3.12 shows the reduction curves of the two zinc-richest 78:22 calcined samples prepared under different calcination atmosphere. Reduction of the sample calcined in 100 % oxygen provides a neat single-peak curve with no distinct dents or shoulders. This is a further indication for a homogenously composed calcined sample to the ones we have already seen in earlier sections. In contrast, the reduction curve of the less homogeneous 78:22 sample calcined in air gives a main single peak as well but shows a distinct plateau as well as visible shoulder at lower temperature, indicative of different types of Cu present in the sample. It is reduced at significantly

higher temperature during the isothermal treatment. The late reduction is another sign of large particles, which compared to nanoparticles tend to react at higher temperatures.

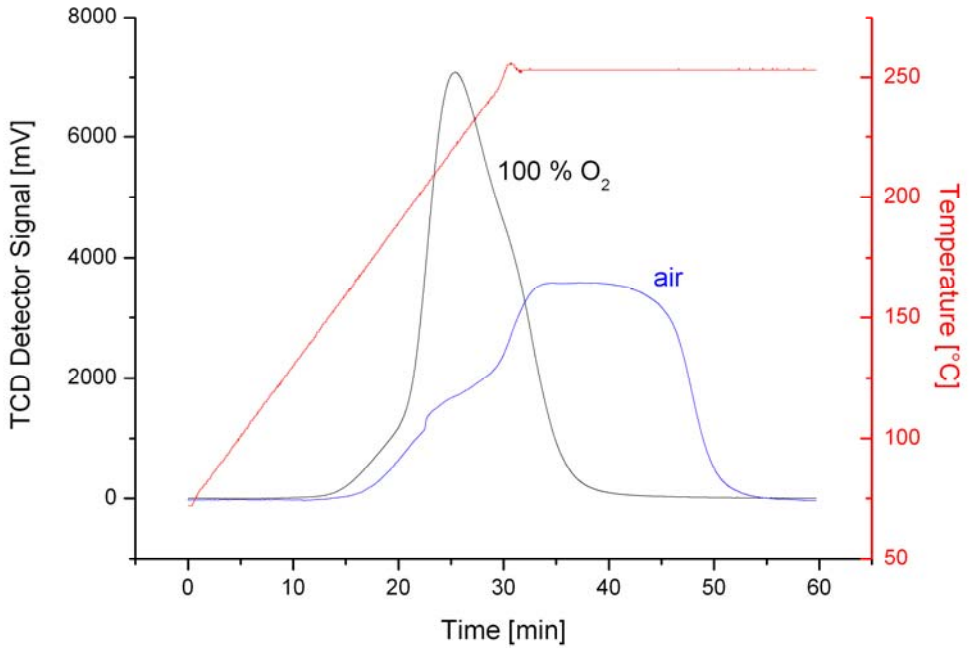

Figure 3.12: Comparison of reduction curves of calcined samples

Finally, a TEM micrograph (see Figure 3.13) shows the finished reduced active catalyst. The arrows point to the needle-type shapes that are still present after reduction, but are now seen at higher magnification compared to the SEM investigation. The distinct particle composition and nano-structuring is apparent in the TEM images. Once again, elemental mapping shown in Figure 3.14 offers insight into the distribution of Cu and Zn in the sample. In this case a relatively homogeneous distribution is achieved, although some areas seem to show no presence of either Cu or Zn.

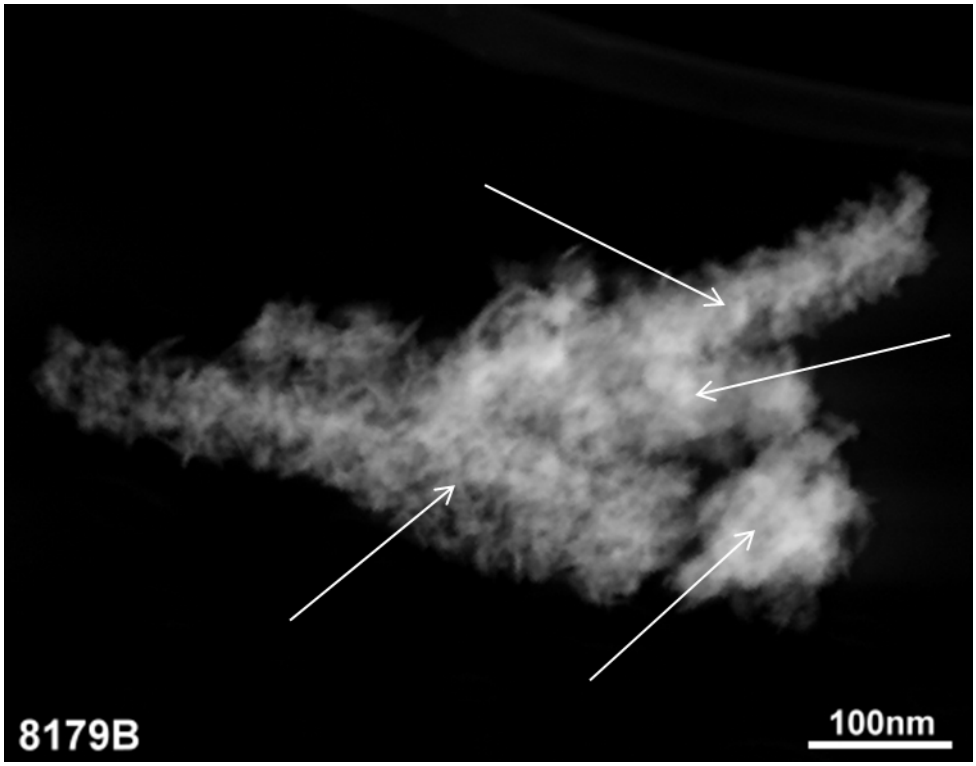

Figure 3.13: TEM micrograph of 78:22 reduced sample

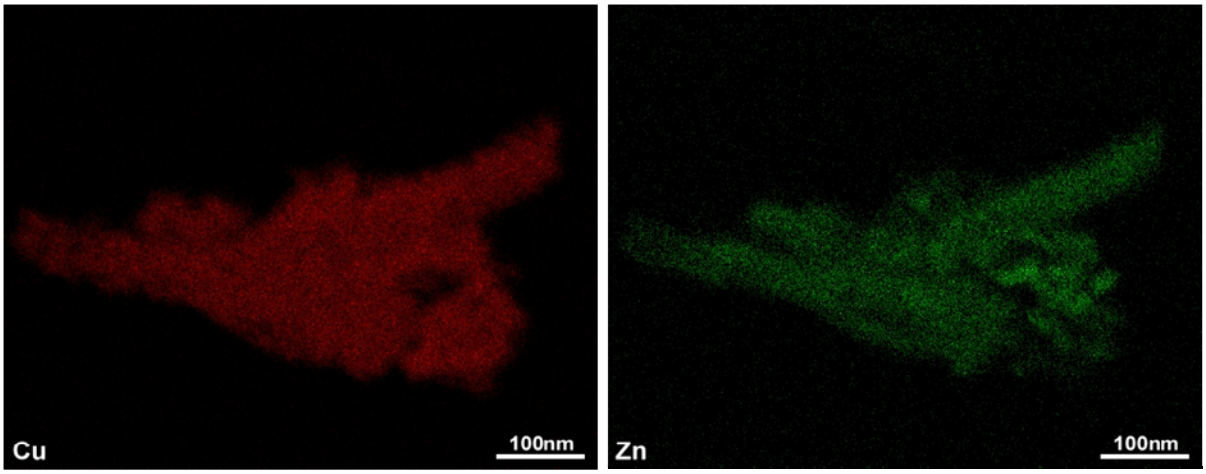

Figure 3.14: Elemental mapping of TEM micrograph in Figure 3.13

4 Conclusion and Outlook

The series of experiments conducted for this work produced promising results. It was shown that formate anions had precipitated together with the metal cations to produce a formate precursor of the formula $(Cu,Zn)_2(OH)_3HCOO$. This material consists of a mixed cation lattice and volatile anions and, thus, is a promising candidate for preparation of Cu/ZnO catalysts for synthesis of methanol. Effective nano-structuring of the precursor can be achieved by mild calcination. The initially needle-like precursor crystals are transformed into porous aggregates of CuO and ZnO nanoparticles. Partial reduction of Cu(II) to Cu(I) was observed when calcination was performed in air. This led to segregation and formation of large Cu_2O particles. This problem could be circumvented by calcination in a more oxidising 100 % O_2 atmosphere.

The resulting sample exhibits homogeneous distribution of Cu and Zn and a surface area of 40 m^2/g. TEM investigations have shown that the nano-particulate microstructure as well as the homogeneous distribution of Cu and ZnO could be conserved during reduction, rendering the basic formate precursor system suitable for preparation of Cu/ZnO catalysts.

Unfortunately, however, the preparation proved to not be fully optimised as indicated by the Cu:Zn ratios, which were found to be much higher than expected from the nominal composition of the starting solutions. The pH chosen for the series was too low – both metals in solution had not fully precipitated. In order for the formate series to fulfil any “green” chemistry potential, full precipitation and transition metal-free mother liquors a prerequisite. Because of this, two parameters were changed in three “outlook” experiments to see which could prove promising for further study.

In the first of these experiments, the reaction pH was increased to 6.5 to ensure that all copper would be precipitated. This, however, yielded aurichalcite, $(Cu,Zn)_5(OH)_6(CO_3)_2$, containing carbonates from the precipitating agent soda. In

other words, pH 6.5 was too high and favoured precipitation of carbonates over formates.

The second experiment was a change of pH to 6.0 while still using sodium carbonate as precipitating agent. However, not all metal was precipitated. Together with XRD analysis showing that the yielded phase was not purely crystalline, this experiment was deemed unsuccessful.

The third experiment, then, was a reaction at pH 6.5 to ensure that all copper would precipitate, using sodium hydroxide as precipitating agent. This eliminated the possibility of yielding aurichalcite as product, too. The result was full precipitation of copper and a yield of formate product, however, the sample did not show particularly good crystallinity.

The results of this paper have set the stage for application of basic formate precursor for preparation of Cu/ZnO catalysts by showing their potential to yield nano-structured and homogeneous materials. However, the important question of the optimal Cu:Zn ratio could not be answered, but the “outlook” experiments have clearly shown that future work on synthesis optimisation will be worthwhile.

5 Experimental

5.1 General Preparation Method

All samples were prepared using the controlled co-precipitation method in a METTLER TOLEDO LABMAX automated laboratory reactor (see Figure 5.1). The mixed metal hydroxy formate precursors were formed from aqueous 0.5 M copper, zinc formate solutions with 1.6 M sodium carbonate solution as precipitating agent. The precipitate was aged in the mother liquor for 30 mins, filtrated, washed until filtrate conductivity < 0.5 mS/cm, dried overnight at 60 °C and then calcined at 225°C (hold time 3 h, ramp rate 2 K/min) to give the metal oxides. The active copper surface was then obtained by reducing the copper oxides to metallic copper over 5 % H_2 in Ar at 250 °C (hold time 30 mins, ramp rate 6 K/min).

Figure 5.1: LabMax automated laboratory reactor

5.2 Methods of Analysis

XRD measurements were carried out with a STOE STADI P transmission diffractometer equipped with a primary focusing germanium monochromator (Cu-$K_{\alpha 1}$ radiation) and linear position sensitive detector. The samples were mounted in the form of small amounts of powder sandwiched between two thin layers of polyacetate film and fixed with a small amount of X-ray amorphous grease.

Full powder pattern fitting and Rietveld crystal structure refinements on the XRD patterns were performed using the software package TOPAS. Crystal structure pictures were created with DIAMOND. ICDD files 5-661 (tenorite), 5-667 (cuprite), 14-687 (gerhardtite), 17-743 (aurichalcite), 36-1451 (zincite) and 41-1390 (malachite), were used for phase identification.

Thermal analyses were carried out with a NETZSCH STA449 thermobalance under a controlled flow of 21 % O_2 in Ar with approximately 20 mg of sample up to 700 °C at a heating rate of 2 K/min. The gases evolved in the thermal analyses were monitored with a quadrupole mass spectrometer (QMS200 OMNISTAR, BALZERS) coupled to the thermal balance via a quartz capillary.

XRF analyses were carried out with a BRUKER PIONEER S4 wavelength dispersive spectrometer using the wax pill technique.

Specific surface areas were determined by N_2 physisorption in a QUANTACHROME AUTOSORB-1 machine; whereby the samples were heated to 80 °C with a hold rate of 2 hours.

Temperature Programmed Reduction (TPR) measurements were carried out on a TPD/R/O 1100 machine from CE INSTRUMENTS by passing 5 vol.% H_2 in Ar at a total flow of 80 ml/min over 50 mg of sample contained in a quartz tube.

SEM images were taken on a HITACHI S-4800 (FEG) system. High resolution TEM images were taken on a PHILIPS CM 200FEG microscope operated at 200 kV.

5.3 Procedure

5.3.1 100:0

For solution 1, 34.04 g malachite was dissolved in 400 ml water with 60.10 ml formic acid (85 wt.%) and filled up to 600 ml to produce 0.5 M metal solution. For solution 2, 169.58 g sodium carbonate was dissolved in 1 l water to produce 1.6 M alkali solution.

400 ml water was placed in LabMax and heated to 65 °C. 600 g solution 1 was continuously added at 20 g/min, while solution 2 was added automatically to keep pH 5.5 constant.

5.3.2 75:25

For solution 1, 6.10 g zinc oxide and 25.53 g malachite were dissolved in 400 ml water with 60.10 ml formic acid (85 wt.%) and filled up to 600 ml to produce 0.5 M metal solution. For solution 2, 169.58 g sodium carbonate was dissolved in 1 l water to produce 1.6 M alkali solution.

400 ml water was placed in LabMax and heated to 65 °C. 600 g solution 1 was continuously added at 20 g/min, while solution 2 was added automatically to keep pH 5.5 constant.

5.3.3 50:50

For solution 1, 12.21 g zinc oxide and 17.02 g malachite were dissolved in 400 ml water with 60.10 ml formic acid (85 wt.%) and filled up to 600 ml to produce 0.5 M metal solution. In order for zinc oxide to completely dissolve, short ultrasound bath at 45 °C was necessary. For solution 2, 169.58 g sodium carbonate was dissolved in 1 l water to produce 1.6 M alkali solution.

400 ml water was placed in LabMax and heated to 65 °C. 600 g solution 1 was continuously added at 20 g/min, while solution 2 was added automatically to keep pH 5.5 constant.

5.3.4 25:75

For solution 1, 18.31 g zinc oxide and 8.51 g malachite were dissolved in 400 ml water with 60.10 ml formic acid (85 wt.%) and filled up to 600 ml to produce 0.5 M

metal solution. In order for zinc oxide to completely dissolve, 30 mins ultrasound bath at 45 °C was necessary. For solution 2, 169.58 g sodium carbonate was dissolved in 1 l water to produce 1.6 M alkali solution.

400 ml water was placed in LabMax and heated to 65 °C. 600 g solution 1 was continuously added at 20 g/min, while solution 2 was added automatically to keep pH 5.5 constant.

5.3.5 0:100

For solution 1, 24.41 g zinc oxide was dissolved in 400 ml water with 60.10 ml formic acid (85 wt.%) and filled up to 600 ml to produce 0.5 M metal solution. In order for zinc oxide to completely dissolve, 2 h ultrasound bath at 45 °C was necessary. For solution 2, 169.58 g sodium carbonate was dissolved in 1 l water to produce 1.6 M alkali solution.

400 ml water was placed in LabMax and heated to 65 °C. 600 g solution 1 was continuously added at 20 g/min, while solution 2 was added automatically to keep pH 5.5 constant.

6 References

[1] Methanol Institute, *http://methanol.org/pdf/wrldsd.pdf* (accessed Aug 31, 2009).

[2] G. A. Olah, A. Goeppert, G. K. Surya Prakash, *Beyond Oil and Gas: The Methanol Economy*. Wiley-VCH, Weinheim, 2006.

[3] U. Onken, A. Behr, *Chemische Prozesskunde – Lehrbuch der Technischen Chemie, 3rd Edition*. Thieme, Stuttgart, 1996.

[4] S. Velu, K. Suzuki, T. Osaki, *Catal. Lett.* **62** (1999) 159.

[5] K.-O. Hinrichsen, J. Strunk, *Nachrichten Chemie* **54** (2006) 1080.

[6] M. V. Twigg, M. S. Spencer, *Appl. Catal. A* **212** (2001) 161.

[7] J.-D. Grunwaldt, A. M. Molenbroek, N.-Y. Topsøe, H. Topsøe, B. S. Clausen, *J. Catal.* **194** (2000) 452.

[8] B. Bems, M. Schur, A. Dassenoy, H. Junkes, D. Herein, R. Schlögl, *Chem. Eur. J.* **9** (2003) 2039.

[9] M. Behrens, D. Brennecke, F. Girgsdies, S. Kißner, A. Trunschke, N. Nasrudin, S. Zakaria, N. F. Idris, S. B. Abd Hamid, B. Kniep, R. Fischer, W. Busser, M. Muhler, R. Schlögl, *Co-precipitation of Mixed Cu, Zn, Al Hydroxycarbonate Precursors for Cu/ZnO/Al_2O_3 Catalysts Investigated by Titration Experiments*, manuscript in preparation.

[10] H. R. Oswald, *Z. Kristallogr. Kristallgeom. Kristallphys. Kristallchem.* **116** (1961) 210.

[11] D. Waller, D. Stirling, F. S. Stone, *Faraday Discuss. Chem. Soc.* **87** (1989) 107.

[12] M. Behrens, F. Girgsdies. A. Trunschke, R. Schlögl, *Eur. J. Inorg. Chem.* **10** (2009) 1347.

[13] M. Schur, B. Bems, A. Dassenoy, I. Kassatkine, J. Urban, H. Wilmes, O. Hinrichsen, M. Muhler, R. Schlögl, *Angew. Chem. Int. Ed.* **42** (2003) 3815.

7 Acknowledgements

Many thanks to Professor Robert Schlögl for giving me the opportunity to work in the Department of Inorganic Chemistry at Fritz-Haber and for agreeing to supervise this project. Sincere thanks also to Professor Jens Beckmann for agreeing to be second supervisor to this project.

A very special thank you to Dr Malte Behrens who warmly welcomed me into the Nanostructure Group and gave me continuous support, especially in the latter stages of completing this work.

I would also like to specially thank Stefan Kißner who was on hand at all times to help and answer all of my questions and with whom it was a pleasure to work.

Many thanks also to Edith Kitzelmann, Dr Nelli Muratova, Gisela Weinberg, Gisela Lorenz, Maike Hashagen, Achim Klein-Hoffmann, Dr Olaf Timpe and Norbert Pfänder for providing the various analytical characterisations.

A special thanks is due to Dr Frank Girgsdies who provided the Rietveld fits of my XRD data, created the images of the unit cells and who was always prepared to pass on his valuable knowledge of crystallography.

Finally, thank you to all the members of the Nanostructure Group for making my time at Fritz-Haber so pleasant.

8 Appendix

8.1 Table of Prepared Samples

Sample #	Cu:Zn Ratio	pH	Precipitating Agent	Preparation Type
7975	50:50 (90:10)	5.5	Na_2CO_3	Precursor
8000	75:25 (96:4)	5.5	Na_2CO_3	Precursor
8045				#7975 calcined in air
8046				#8000 calcined in air
8059	25:75 (78:22)	5.5	Na_2CO_3	Precursor
8064	0:100 (0:100)	5.5	Na_2CO_3	Precursor
8105				#8059 calcined in air
8108				#8064 calcined in air
8110	50:50 (50:50)	6.5	Na_2CO_3	Precursor
8141	100:0 (100:0)	5.5	Na_2CO_3	Precursor
8163	50:50 (54:46)	6.5	NaOH	Precursor
8164	50:50 (63:37)	6.0	Na_2CO_3	Precursor
8166				#8141 calcined in air
8176				#8059 calcined in 100 % O_2
8179				#8176 reduced
8256				#8105 reduced